

RT-cache: Efficient Robot Trajectory Retrieval System

Owen Kwon¹, Abraham George², Alison Bartsch², and Amir Barati Farimani^{1,2}

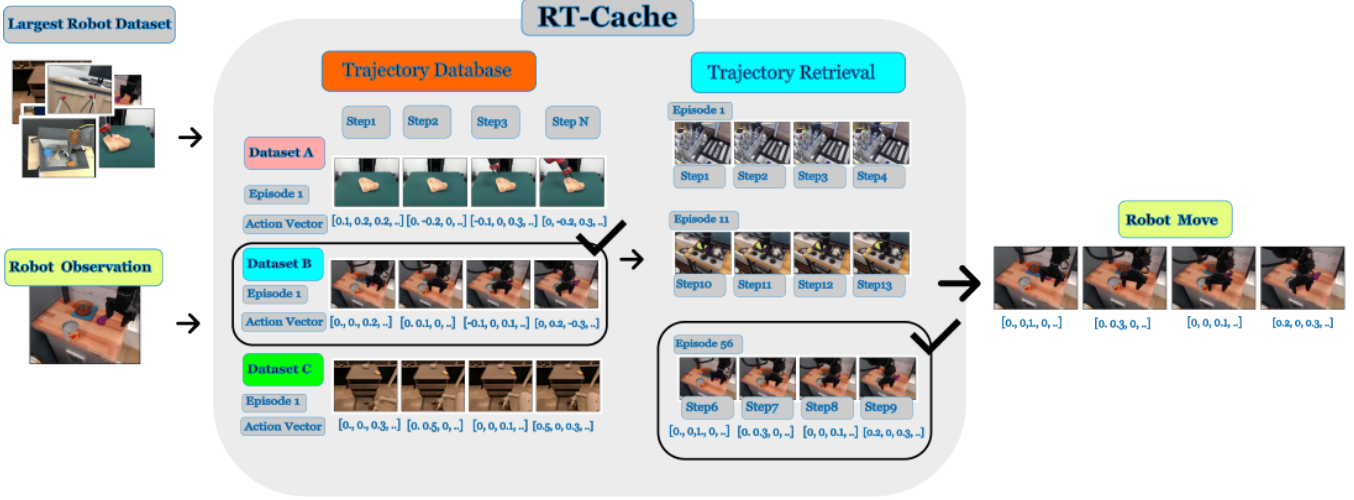


Fig. 1: **RT-Cache Overview.** *Left:* We construct a multi-dataset trajectory *Memory* by embedding image–action pairs into a shared vector space, creating a broad repository of real-world experiences. *Right:* At runtime, the current camera frame is mapped into that space to retrieve the top- K most similar snippets. The best match (green outline) is replayed for the next N steps, sidestepping repeated Vision–Language–Action inferences. Dashed arrows illustrate the closed retrieval loop.

Abstract—This paper introduces RT-cache, a novel *trajectory-memory pipeline* that accelerates real-world robot inference by leveraging *big-data retrieval* and *learning from experience*. While modern Vision–Language–Action (VLA) models can handle diverse robotic tasks, they often incur high per-step inference costs, resulting in significant latency, sometimes minutes per task. In contrast, RT-cache stores a large-scale *Memory* of previously successful robot trajectories and *retrieves* relevant multi-step motion snippets, drastically reducing inference overhead. By integrating a *Memory Builder* with a *Trajectory Retrieval*, we develop an efficient retrieval process that remains tractable even for extremely large datasets. RT-cache flexibly accumulates real-world experiences and replays them whenever the current scene matches past states, adapting quickly to new or unseen environments with only a few additional samples. Experiments on the Open-X Embodiment Dataset and other real-world data demonstrate that RT-cache completes tasks both faster and more successfully than a baseline lacking retrieval, suggesting a practical, data-driven solution for real-time manipulation.

Keywords: Big Data, Robot System, Learning from Experience

I. INTRODUCTION

Recently, *Vision–Language–Action* (VLA) models have enabled remarkable progress in robot control by providing

a single, generalized framework for perception and action [1]–[5]. Despite their versatility, these models often suffer from high inference overhead in real-world settings, as each step in a robot’s trajectory may require a large forward pass. Although techniques such as parallel decoding [5] can significantly accelerate iterative generation, large model computations are still needed at every step, thereby restricting deployment in real-time or near-real-time scenarios, including humanoid robotics.

To address these computational bottlenecks, we draw inspiration from how humans naturally accelerate repeated tasks by recalling past experiences. This concept, sometimes referred to as the *Replay of Problem Solving Episodes* [6], suggests that a “memory” of previously successful trajectories can serve as a retrieval-based cache. Whenever the current scene closely resembles a previously solved instance, the robot can simply replay the stored multi-step trajectory, thus reducing the number of inferences needed. This principle mirrors how repetition makes chores faster and more efficient over time.

We therefore propose the *RT-cache pipeline* as a practical mechanism for real-world inference. Rather than relying on step-by-step outputs from a VLA model, our approach maintains a comprehensive *Memory Database* of trajectories, images, and partial text annotations. At runtime, a retrieval

¹Department of Biomedical Engineering, Carnegie Mellon University, Pittsburgh PA 15213, USA.

²Department of Mechanical Engineering, Carnegie Mellon University, Pittsburgh PA 15213, USA.

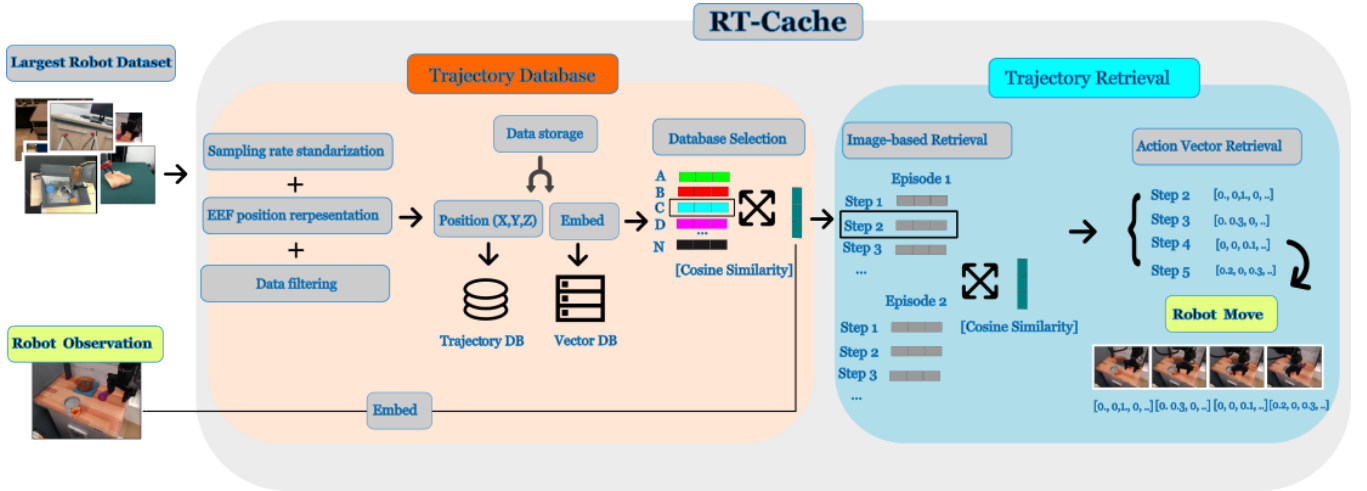


Fig. 2: **RT-Cache retrieval—from terabytes to real time.** (1) **Trajectory Database:** We unify and standardize diverse logs by converting actions to a consistent representation, then embed each image–action pair in a vector database. An efficient data-partitioning strategy keeps retrieval tractable at massive scale. (2) **Trajectory Retrieval:** For every new robot observation, we select a relevant subset of the database (e.g., via centroid filtering and sub-sampling), perform an image-based k -NN search, and replay the top- K closest motion snippets on the robot. This avoids repeated Vision–Language–Action inferences while adapting to new scenes in real time.

module compares the latest image (and optionally text) embeddings to find the best-matching snippet. By replaying that snippet for the next several steps, the system sidesteps repeated calls to a large generative model, substantially reducing overall inference time. In contrast to traditional action-planning pipelines that depend on *hand-designed* motion primitives or heuristics, RT-cache taps into a growing corpus of real robot experiences, dynamically adapting to new tasks and scenarios without requiring domain-specific engineering.

Contributions.

- We introduce **RT-cache**, a retrieval-based pipeline that combines a *Memory Builder* and a *Trajectory Retrieval* to select multi-step actions from a large repository of real-robot experiences.
- We propose a **multi-stage retrieval strategy**—data selection strategy (centroid filtering or sub-sampling) and final k -NN search—to keep lookup times tractable for extremely large datasets with millions of embedded states.
- We validate RT-cache in real-world settings (including the Open-X Embodiment Dataset), showing **faster average operation time** and **stable or improved success rates** compared to a baseline Vision–Language–Action model [5].

II. RELATED WORKS

A. Vision-Language-Action (VLA) Models in Robotics

Recent advances in *Vision-Language-Action* (VLA) models [1]–[5] demonstrate strong generalization to out-of-distribution conditions and novel semantic concepts, surpassing earlier vision foundation models [7]–[12]. In particular, [1] proposed LoRA-based finetuning for single-arm robots

at low control frequencies (10 Hz), while [5] introduced an adaptation strategy—including parallel decoding—for fast inference on a bimanual manipulator at higher frequencies (25–50+ Hz).

Despite these advances, VLA models generally require substantial finetuning efforts, demanding additional data, computational resources, and time. Moreover, each new task setting may necessitate further finetuning or calibration, raising concerns about overwriting previously learned capabilities [13]. These repeated finetuning and inference steps can significantly increase resource requirements, underscoring the need for more efficient approaches to deploying large models in robotic systems.

B. Action Reuse and Retrieval-Based Planning

Traditional action-planning pipelines often rely on *hand-engineered motion primitives* or *cached policies* [14]–[16] to streamline repetitive tasks such as pick-and-place. While these techniques can be effective for well-defined scenarios, their reliance on manually designed primitives makes them difficult to extend to new or more intricate manipulations.

Another important direction is *imitation learning*, which leverages human demonstrations to learn complex skills [8], [9], [17]–[23]. Although methods like VINN [24] have shown promise in generalizing to unseen environments, they typically do not address large-scale image retrieval across massive, multi-task datasets. As these datasets continue to grow in size and diversity [25], efficiently identifying and reusing relevant past experiences becomes increasingly important.

In contrast, our pipeline explicitly integrates *retrieval* from vast real-robot datasets to select multi-step motion snippets. By accumulating a large repository of past trajectories, we

TABLE I: **Representative sub-datasets in the Open-X Embodiment corpus.** Each row shows how the original logging frequency, action space, and units (“Before”) were converted (“After”) to a 10 Hz Cartesian end-effector format, standardizing diverse data (e.g., position, velocity, joint space) into a consistent 7-D EEf representation.

Dataset	Before			After (Unified)		
	Freq. (Hz)	Action Space	Units	Freq. (Hz)	Action Space	Comments
fractal20220817_data	3	EEf pos. (Cart.)	m (x,y,z)	10	EEf pos. (Cart.)	Upsampled (linear)
kuka	10	EEf pos. (Cart.)	m (x,y,z)	10	EEf pos. (Cart.)	—
bridge	5	EEf pos. (Cart.)	m (x,y,z)	10	EEf pos. (Cart.)	Upsampled
berkeley_cable_routing	10	EEf vel. (Cart.)	m/s (x,y,z)	10	EEf pos. (Cart.)	Vel. \rightarrow pos. (0.1 s)
roboturk	10	EEf pos. (Cart.)	m (x,y,z)	10	EEf pos. (Cart.)	—
nyu_door_opening_surprising_effect...	3	EEf pos. (Cart.)	m (x,y,z)	10	EEf pos. (Cart.)	Upsampled
viola	20	EEf pos. (Cart.)	m (x,y,z)	10	EEf pos. (Cart.)	Downsampled
berkeley_autolab_ur5	5	EEf pos. (Cart.)	m (x,y,z)	10	EEf pos. (Cart.)	Upsampled
columbia_cairlab_pusht_real	10	EEf pos. (Cart.)	m (x,y,z)	10	EEf pos. (Cart.)	—
austin_sirius_dataset_converted...	20	EEf vel. (Cart.)	m/s (x,y,z)	10	EEf pos. (Cart.)	Downsample + vel \rightarrow pos
austin_sailor_dataset_converted...	20	EEf vel. (Cart.)	m/s (x,y,z)	10	EEf pos. (Cart.)	Same as above
utokyo_xarm_pick_and_place_convert...	10	EEf pos. (Cart.)	m (x,y,z)	10	EEf pos. (Cart.)	—
tokyo_u_ismmo_converted...	10	EEf vel. (Cart.)	m/s (x,y,z)	10	EEf pos. (Cart.)	Vel. \rightarrow pos.
dlr_sara_pour_converted...	10	EEf vel. (Cart.)	m/s (x,y,z)	10	EEf pos. (Cart.)	Vel. \rightarrow pos.
dlr_sara_grid_clamp_converted...	10	EEf vel. (Cart.)	m/s (x,y,z)	10	EEf pos. (Cart.)	Vel. \rightarrow pos.
dlr_edan_shared_control_converted...	5	EEf pos. (Cart.)	m (x,y,z)	10	EEf pos. (Cart.)	Upsampled
asu_table_top_converted...	12.5	EEf pos. (Cart.)	m (x,y,z)	10	EEf pos. (Cart.)	Downsampled
stanford_robotcook_converted...	5	EEf pos. (Cart.)	m (x,y,z)	10	EEf pos. (Cart.)	Upsampled
utaustin_mutex	20	EEf pos. (Cart.)	m (x,y,z)	10	EEf pos. (Cart.)	Downsampled

can replay entire action segments rather than inferring each step from scratch, thereby reducing repeated computation. As this memory expands, the system more readily finds and reuses solutions with minimal reliance on expensive model inferences. This approach effectively combines the broad applicability of large VLA models with a retrieval mechanism that mitigates per-step computational overhead.

III. METHODS

This section details our approach for real-time robot control. We first describe how we build a large-scale, unified dataset from the diverse trajectories in the Open-X Embodiment collection [25]. We then present the *RT-Cache Pipeline*, a retrieval-based framework that leverages this unified dataset to accelerate multi-step action selection in real-world environments.

A. Building a Unified Dataset Collection

1) *Open-X Embodiment*: Our work leverages the Open-X Embodiment dataset, which includes over one million real-robot trajectories from 22 platforms (single-arm to bi-manual and quadrupeds). Contributed by 34 labs worldwide, these 60 sub-datasets use RLDS format [1] and span diverse action spaces (Cartesian vs. joint) and sensor modalities (RGB, depth, point clouds).

2) *Dataset Processing*: The Open-X dataset spans control frequencies from 3 Hz to 30 Hz and includes actions expressed in position, velocity, or joint-space commands. To ensure uniformity, we adopt a three-step *unification* procedure:

- 1) **Sampling rate standardization**: Convert all trajectories to 10 Hz. Lower-frequency data are linearly interpolated, while higher-frequency data are subsampled.
- 2) **EEf position representation**: Represent every action as an end-effector (EEf) position in Cartesian space. For velocity-based datasets (e.g., 0.2 m/s), integrate

each velocity over 0.1 s to approximate positional displacement.

- 3) **Filtering by action shape**: Exclude any episodes lacking a 7-D action shape or those using only joint-space commands.

This standardization process yields a consistent, 7-D Cartesian action representation across all sub-datasets, simplifying subsequent retrieval tasks.

3) *Database Setup*: We adopt a **two-tiered database strategy** to efficiently store raw robot data alongside high-dimensional embeddings:

a) *MongoDB for Raw Data.*: We use MongoDB to store time-step information (e.g., timestamps, unified 7-D actions, RGB frames). Each entry corresponds to a single step, indexed by (*episode_id*, *step_id*) for rapid lookups and flexible filtering.

b) *Vector Database for Embeddings.*: For similarity-based retrieval, we maintain a separate *vector database* (Qdrant). We compute and store one embedding per state:

- **DINOv2 [26] image features** (1024-dimensional)
- **SigLIP [27] image features** (1152-dimensional)

We concatenate these features into a single 2176-dimensional vector, which empirically outperforms either encoder alone. At query time, the incoming camera frame is embedded similarly, and a top-*K* nearest-neighbor search (e.g., via cosine distance) retrieves the most relevant states.

The vector database returns candidate state IDs, which map back to MongoDB records for the corresponding raw data. This separation between *similarity lookup* (in the vector DB) and *record storage* (in MongoDB) allows our system to scale to millions of states without compromising retrieval speed.

B. RT-Cache Pipeline

1) *Overall Retrieval-Based Pipeline*: Our system converts each new camera image into a high-dimensional embedding

and uses it to query a large database of prior robot experiences for candidate actions. The retrieval pipeline proceeds in four main stages, each with defined parameters:

a) *Stage 1: Embedding the Current Observation:*

- Let I_t be the current RGB frame at time t .
- We feed I_t through two pretrained encoders, DINOv2 and SigLIP, yielding feature vectors $\mathbf{d}_t \in \mathbb{R}^{1024}$ and $\mathbf{s}_t \in \mathbb{R}^{1152}$, respectively.
- We then concatenate and ℓ_2 -normalize these vectors to form a single **target embedding**:

$$\mathbf{e}_t = \text{Norm}([\mathbf{d}_t \parallel \mathbf{s}_t]), \quad (1)$$

where $[\cdot \parallel \cdot]$ denotes vector concatenation and $\text{Norm}(\cdot)$ denotes ℓ_2 -normalization.

b) *Stage 2: Database Selection:* A naive search over billions of embeddings is computationally infeasible, so we employ two different filtering steps that drastically narrow down the candidate space before a final k -nearest-neighbor query:

- 1) **Dataset-Centroid Stage.** We partition the entire Open-X corpus by dataset (e.g., each lab’s subset). For dataset d , we precompute a centroid \mathbf{c}_d by averaging all embeddings within that dataset:

$$\mathbf{c}_d = \frac{1}{N_d} \sum_{i=1}^{N_d} \mathbf{f}_{d,i}, \quad d = 1, 2, \dots, D, \quad (2)$$

where $\mathbf{f}_{d,i} \in \mathbb{R}^{2176}$ is the i -th embedding and N_d is the total number of embeddings in dataset d . At query time, we compute the distance (e.g., cosine distance) between the target embedding \mathbf{e}_t and each centroid \mathbf{c}_d , then select the top m datasets whose centroids are closest:

$$d_{1:m}^* = \arg \min_{d \in \{1, \dots, D\}} \text{dist}(\mathbf{e}_t, \mathbf{c}_d). \quad (3)$$

- 2) **Small Subset Stage.** For each of these m shortlisted datasets, we *randomly sample* (or *cluster-sample*) a small subset of size S (e.g., a few thousand) to form a local index. We then perform a finer-grained k -nearest-neighbor (k -NN) search on each local index using \mathbf{e}_t , retrieving the top candidates from each.

This hierarchical filtering limits retrieval to $\mathcal{O}(m \times S)$ embeddings rather than $\mathcal{O}(\sum_d N_d)$, greatly speeding up queries.

c) *Stage 3: Similarity Computation and Candidate Selection:* After pooling the candidates from all local indices, we calculate *cosine similarity* between the target embedding \mathbf{e}_t and each candidate embedding \mathbf{f}_j :

$$\text{sim}(\mathbf{e}_t, \mathbf{f}_j) = \frac{\mathbf{e}_t \cdot \mathbf{f}_j}{\|\mathbf{e}_t\| \|\mathbf{f}_j\|}. \quad (4)$$

We rank the candidates by similarity and select the top K (e.g., $K = 50$). Let $\{\mathbf{f}_j\}_{j=1}^K$ denote these final neighbors.



Fig. 3: **Multi-camera test arena and success criterion.** A 7-DoF Franka Emika Panda manipulator operates on a tabletop observed by three Intel RealSense D415 cameras: a *Side Cam*, a wide-angle *Front Cam*, and a *Wrist Cam*. One of three objects—a water bottle, mug, or bowl—is placed at a location before each rollout. A trial is deemed *Successful* when the end-effector reaches the object’s graspable region, as illustrated by the terminal frames on the right.

d) *Stage 4: Retrieval and Action Execution:* Each embedding \mathbf{f}_j maps to a database record containing a *trajectory snippet*, i.e., the next N actions $\mathbf{a}_{t:t+N}^{(j)}$. We consider two approaches:

- **Single Best Neighbor:** Use only the highest-scoring neighbor j^* and retrieve $\mathbf{a}_{t:t+N}^{(j^*)}$, executing these N actions with no further inference calls.
- **Averaged Actions (Multi-Neighbor):** Compute an average of actions from the top K neighbors:

$$\bar{\mathbf{a}}_{t:t+N} = \frac{1}{K} \sum_{j=1}^K \mathbf{a}_{t:t+N}^{(j)}, \quad (5)$$

which can reduce noise if multiple neighbors are closely related.

C. Experimental Setup

We evaluate RT-cache on a simplified manipulation task where a 7-DoF Franka Emika Panda robot moves its end-effector (EEF) toward a specific object placed on a tabletop. Three Intel RealSense D415 cameras provide different views of the workspace: a lateral **Side Cam**, a wide-angle **Front Cam**, and a **Wrist Cam** mounted on the robot arm (Fig. 3). We randomly place three objects—a plastic bottle, a ceramic mug, and a plastic bowl—at varied positions. A trial is deemed *Successful* if the EEF is within the object’s graspable region by the final step.

TABLE II: **Comparison of success rates (%) and operation times (s) for multiple objects and camera placements.** Rows distinguish systems (e.g., RT-Cache vs. OpenVLA-OFT [5]) and approaches (e.g., zero-shot vs. few-shot). For each object (Bowl, Cup, Bottle) and camera (Front, Left, Right), we report success rate (%) and operation time (s). *Total* columns average the three camera views, and *Overall* rows average across objects. Dashes (–) indicate no data or not applicable.

System	Approach	Object	Success Rate (%)				Operation Time (s)			
			Front	Left	Right	Total	Front	Left	Right	Total
RT-Cache (Ours)	Zero-shot	All	0	0	0	0	–	–	–	–
	Few-shot (wrist cam)	Bowl	100	100	100	100	65	63	54	61
		Cup	100	100	100	100	64	73	67	68
		Bottle	100	67	100	89	76	63	66	68
		<i>Overall</i>	—	—	—	96	—	—	—	66
	Few-shot (3 rd -side)	Bowl	100	100	33	78	43	52	93	63
		Cup	67	0	0	22	91	–	–	91
		Bottle	67	0	100	56	78	–	78	78
		<i>Overall</i>	—	—	—	52	—	—	—	77
	Few-shot (3 rd -front)	Bowl	100	100	33	78	65	64	50	60
		Cup	100	100	100	100	65	64	66	65
		Bottle	100	100	100	100	64	61	62	63
		<i>Overall</i>	—	—	—	93	—	—	—	63
OpenVLA-OFT [5]	Zero-shot	All	0	0	0	0	–	–	–	–
	Fine-tuned	All	0	0	0	0	–	–	–	–
	–	<i>Overall</i>	—	—	—	0	—	—	—	—

a) Scenarios: We test two setups to gauge RT-cache’s adaptability:

- **Zero-Shot:** No in-domain data exist for the specific object/camera/pose combination, so we check if purely visual similarity can retrieve a relevant multi-step snippet.
- **Few-Shot:** We add up to 27 short demonstration episodes (each ~ 15 steps) capturing the new scene. This tests how minimal in-domain examples boost retrieval accuracy.

b) Data Collection: We recorded short trajectories involving 2–3 objects placed at different table locations (left, right, front, back), with each step logging:

- A **3D Cartesian** action vector (EEF translation),
- A **single wrist or third-person** camera image.

These (action, image) pairs form the fine-tuning dataset, ensuring alignment between the VLA model and our retrieval pipeline.

c) Fine-Tuning Details.: Starting from a pretrained OpenVLA-OFT checkpoint, we apply Low-Rank Adaptation (LoRA) with:

- **LoRA rank:** 32,
- **Learning rate:** 5×10^{-4} (decayed after 100 k steps),
- **Max steps:** 150 000,
- **Camera view:** a single third-person viewpoint.

After $\sim 150\,000$ training iterations, the model’s representations stabilize across multiple objects and camera angles.

IV. RESULTS AND DISCUSSION

We now present our quantitative and qualitative findings for **RT-cache**, comparing it against a standard Vision-

Language-Action (VLA) baseline. After reporting core performance metrics, we analyze how horizon length (i.e., the number of future steps) and small in-domain samples affect success. We then discuss system efficiency and highlight common failure cases.

A. Success Rate and Operation Time

Table II summarizes two primary metrics:

- 1) *Success Rate:* Whether the robot’s end-effector (EEF) is within the target object’s graspable region by the final step.
- 2) *Operation Time:* The wall-clock duration to complete the episode.

We consider three objects (cup, bowl, bottle) under three camera placements (front, side, wrist).

a) Comparison to Baseline.: Although OpenVLA-OFT [5] employs a parallel decoding approach for substantial speedups, our limited fine-tuning dataset (460 steps) poses a significant challenge for robust adaptation. While improved performance might be achievable with more data or advanced tuning strategies, such approaches typically require expert domain knowledge and carefully curated data, which can be prohibitive in real-world deployments. In contrast, **RT-cache** consistently attains success rates on par with—or higher than—the OpenVLA-OFT baseline across all viewpoints. Furthermore, by replaying multi-step snippets, it avoids per-step model calls and substantially accelerates execution, especially in tasks requiring frequent corrective adjustments.

b) Effect of Adding a Single Sample.: Introducing even *one* new, relevant demonstration per camera can dramatically boost success for failure cases in the zero-shot condition (e.g., side-camera scenarios with 0% success). Thus, even

TABLE III: **Performance under different snippet horizons.** Rows indicate horizon lengths $N \in \{1, 3, 5\}$, grouped by camera perspective (Wrist, 3rd-Person Side, 3rd-Person Front). Columns show success rates (%) and average operation times (s) for Front, Left, and Right viewpoints, with “Avg” denoting the aggregate.

N	Success Rate (%)				Operation Time (s)			
	Avg	Front	Left	Right	Avg	Front	Left	Right
Wrist Camera								
1	85	100	89	67	65	68	65	62
3	96	100	89	100	66	69	67	62
5	67	89	33	78	70	69	61	77
3rd-Person Side Camera								
1	33	44	11	44	72	72	39	79
3	52	78	33	44	68	67	53	82
5	22	33	0	33	70	68	—	73
3rd-Person Front Camera								
1	78	67	89	78	65	66	64	66
3	93	100	100	78	63	65	63	62
5	44	44	44	44	73	83	63	73

minimal extra data can establish stronger retrieval anchors, enabling the system to find suitable snippets from visually similar states. In practice, we observed that a single well-chosen snippet can re-align the entire search for a given viewpoint.

B. Impact of Future-Horizon Length

Table III examines how choosing a horizon $N \in \{1, 3, 5\}$ affects both success and average time per trial.

a) Short Horizons ($N = 1$): When $N = 1$, the robot re-queries the database on every step, quickly adapting to environmental changes but adding overhead from frequent lookups. This overhead can slightly slow completion times, despite each step being optimally matched.

b) Moderate Horizons ($N = 3$): A horizon of $N = 3$ typically balances speed and accuracy. Retrieval occurs once every three steps, reducing overhead while still reacting if, for instance, an object is nudged mid-episode.

c) Long Horizons ($N = 5$): For static scenes, $N = 5$ can converge faster by replaying longer snippets with fewer interruptions. However, if the snippet mismatches the current scene, the robot may loop or overshoot, highlighting a need for dynamic re-querying when objects move unexpectedly.

C. System Efficiency and GPU Usage

Table IV details resource usage for RT-cache versus OpenVLA-OFT. RT-cache requires only ~ 8 – 10 GB of GPU memory, relying on a fast vector database for embedding retrieval. However, storing ~ 95 GB of image embeddings and ~ 3.1 GB of metadata requires around 100 GB of disk space—a trade-off that significantly reduces large-model inferences, which otherwise dominate GPU usage in standard VLA pipelines.

TABLE IV: **Estimated resource usage per runtime configuration.** We list approximate GPU memory usage, disk requirements, and fine-tuning times for our pipeline vs. OpenVLA-OFT. Fine-tuning OpenVLA-OFT typically takes 10 h and 15 GB of checkpoint storage; safety experiments may reach 100 GB.

Configuration	GPU memory	External disk	Fine-tune time
Our Pipeline	8 GB to 10 GB	~ 100 GB ¹	—
OpenVLA-OFT Model	16 GB to 24 GB	15 GB (per checkpoint)	10 h

By contrast, fully finetuning and running OpenVLA-OFT can demand 16–24 GB of GPU memory and up to 100 GB in disk space for specialized experiments. RT-cache thus shifts the bottleneck primarily to disk I/O, enabling real-time inference on more modest hardware.

D. Improved Pipeline Speed

Table V compares retrieval times for different database-selection strategies. An exhaustive nearest-neighbor search over millions of embeddings can take minutes, effectively making real-time tasks impossible [24]. In practice, traditional systems might time out because they are not designed for massive datasets.

Instead, our strategy completes lookups in under one second, even on large corpora, keeping RT-cache practical for real-world deployments where every second matters—such as human–robot collaborative settings.

TABLE V: **Operation times for different database-selection strategies.** A naive full-database query can exceed 300 s, making real-time usage infeasible. In contrast, our sampling both complete in about 0.1 s on the same corpus, enabling real-time retrieval.

Selection Method	Operation Time
Full-DB Search	Time-out (> 300 s)
Dataset-Centroid Stage	~ 0.1 s
Small Subset Stage	~ 0.1 s

E. Discussion

1) How Does Retrieval Scale with Database Coverage?: The results in Table II show that multi-step retrieval effectively replaces costly repeated model calls and reduces task time. These findings underscore the importance of *database coverage*: having at least a few examples for each camera viewpoint and object arrangement is crucial to stable retrieval. Even a single new snippet can fix entire failure classes (e.g., side-camera views of the mug).

2) What Are Common Failure Modes, and How Can We Mitigate Them?: Figure 5 illustrates typical errors, such as minor positional offsets or incorrect gripper orientation. These near-misses often occur when an object is partially occluded or the snippet comes from a slightly different pose.

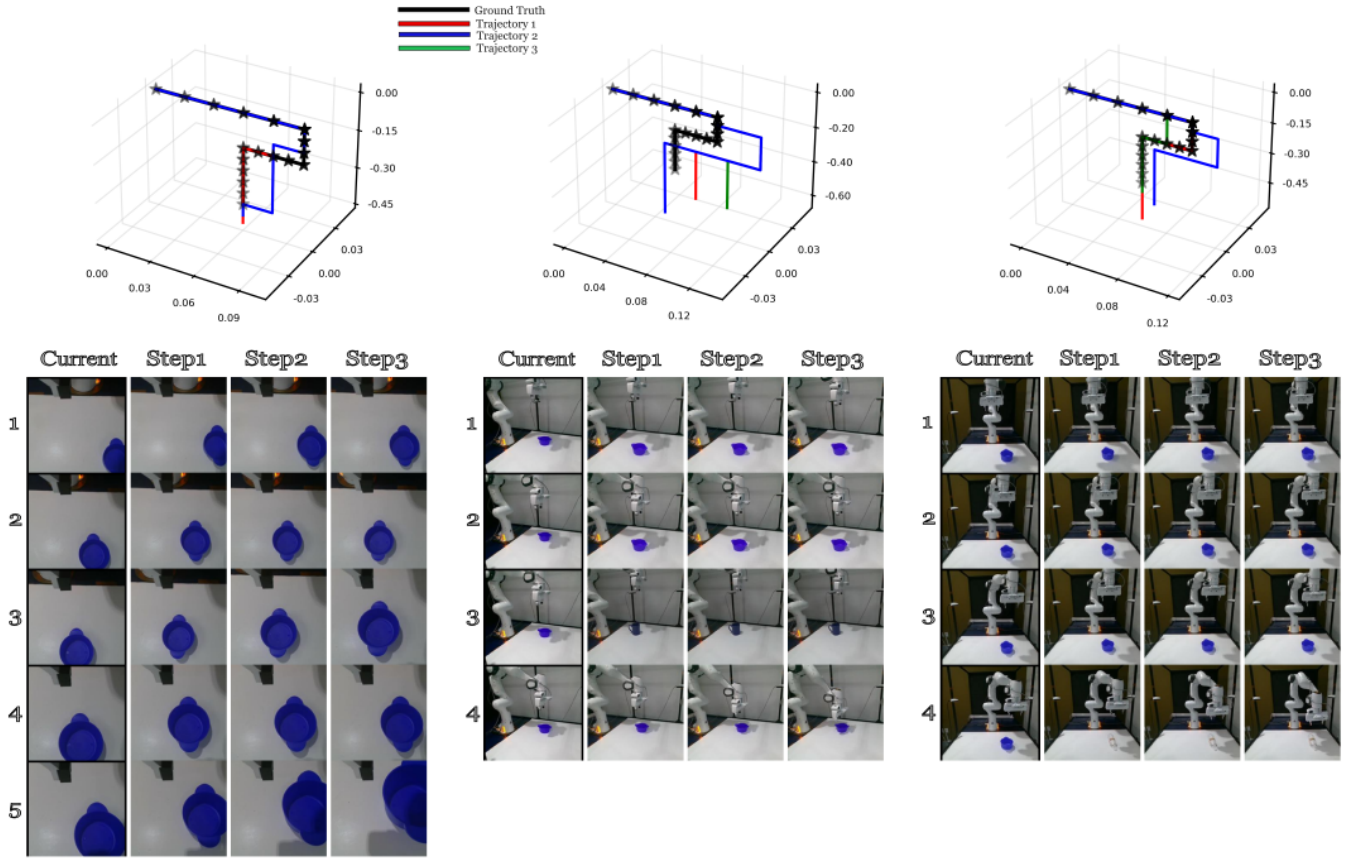


Fig. 4: **Scalability and example retrievals.** *Top:* 3D plots compare a ground-truth trajectory (black) with three retrieved motion snippets (colored lines) under different camera viewpoints, illustrating minor variations in length or shape. *Bottom:* Each row depicts a retrieved snippet from its initial “current” frame to subsequent steps, demonstrating how RT-cache aligns retrieval with each camera perspective (wrist, side, or front). Despite a growing memory (millions of states), retrieval remains sub-linear in time thanks to hierarchical selection.

Another challenge arises when the environment changes mid-execution (e.g., someone moves the bowl). Since RT-cache replays a snippet for up to N steps, unmodeled scene shifts can cause collisions or overshoot. More frequent retrieval queries or auxiliary sensing (e.g., force feedback) could mitigate these issues.

3) How Similar Is the Retrieved Path to the Original?:

- **Section A.1 (Three Trajectories).** Figure 4 shows that each snippet (e.g., from the wrist-cam) targets the same object and viewpoint but can diverge slightly, much like a human “repeating” a skill with minor variations. This illustrates how our pipeline focuses on *functionally* correct paths rather than exact replicas.
- **Section A.2 (Similarity to Original).** While some replayed paths are longer or shorter, they stay close enough to the ground-truth trajectory (black line) to fulfill the intended goal (e.g., achieving a stable grasp).
- **Section B.1 (Next-Step Retrieval).** The bottom images sequence each snippet from its “current” state onward, highlighting how RT-cache continuously selects forward-looking frames in line with the camera view.
- **Section B.2 (Viewpoint-Specific Retrieval).** The sys-

tem retrieves snippets aligned with the active camera: wrist-cam queries yield wrist-cam snippets, side-cam queries yield side-cam snippets, and so forth. This viewpoint consistency substantially improves retrieval accuracy in our trials.

4) *How Does Horizon Length Balance Speed and Adaptation?:* From Table III, short horizons ($N = 1$) enable continuous correction but add overhead from repeated retrieval calls, whereas longer horizons ($N = 5$) risk errors if a snippet is poorly matched. In many practical scenarios, $N = 3$ provides a good trade-off. Future work could explore dynamic horizon selection, where the snippet length is automatically adjusted based on real-time confidence or scene changes.

V. LIMITATIONS AND FUTURE DIRECTIONS

a) *Image-Only Retrieval.*: While our approach matches image embeddings to retrieve multi-step actions, relying solely on visual similarity can be limiting. Future directions include incorporating additional feedback signals, such as human annotations via Reinforcement Learning from Human Feedback (RLHF) [28] or high-level textual cues (e.g.,



Fig. 5: **Typical failure cases.** (A) The arm halts just short of the mug’s graspable region. (B) The retrieved snippet steers the gripper too far right of the water bottle. (C) Another snippet overshoots left of the same bottle. (D) The gripper descends beyond the bowl’s rim, missing the target height.

“grasp the bottle on the right”), to refine snippet selection. Integrating *action requirements* (e.g., language or state embeddings) could further disambiguate visually similar scenes. Moreover, adopting *active perception* strategies [29] and incorporating common-sense reasoning [16] may help the robot gather pertinent information, thereby improving retrieval quality for tasks that demand nuanced context.

b) Expanded Experimental Setup.: Although we focus on a single-arm manipulation scenario with a limited set of objects, broader evaluations are needed to fully gauge generalization and robustness. Future work will explore multi-object tasks, varying shapes and materials, and cluttered environments. Such tests will reveal the pipeline’s performance boundaries under more diverse conditions and guide domain-specific optimizations.

VI. CONCLUSIONS

We presented *RT-Cache*, a trajectory-memory pipeline that drastically reduces per-step inference costs by retrieving and reusing relevant trajectories from a large-scale robotic dataset. This approach embodies the principle of *learning from experience*, enabling tasks to be completed in a fraction of the time required by baseline Vision–Language–Action (VLA) models. While our experiments primarily focused on a grasp-like task, the pipeline is broadly applicable and can be integrated with standard humanoid controllers or higher-level planning frameworks. Ultimately, our aim is to bolster the real-world viability of big-data-driven robot systems, bridging the gap between the representational power of large

VLA models and the stringent latency requirements of real-time operations.

REFERENCES

- [1] M. J. Kim, K. Pertsch, S. Karamcheti, T. Xiao, A. Balakrishna, S. Nair, R. Rafailov, E. Foster, G. Lam, P. Sanketi *et al.*, “Openvla: An open-source vision-language-action model,” *arXiv preprint arXiv:2406.09246*, 2024.
- [2] K. Black, N. Brown, D. Driess, A. Esmail, M. Equi, C. Finn, N. Fusai, L. Groom, K. Hausman, B. Ichter *et al.*, “ π_0 : A vision-language-action flow model for general robot control,” *arXiv preprint arXiv:2410.24164*, 2024.
- [3] A. Brohan, N. Brown, J. Carbajal, Y. Chebotar, X. Chen, K. Choremanski, T. Ding, D. Driess, A. Dubey, C. Finn *et al.*, “Rt-2: Vision-language-action models transfer web knowledge to robotic control,” *arXiv preprint arXiv:2307.15818*, 2023.
- [4] O. M. Team, D. Ghosh, H. Walke, K. Pertsch, K. Black, O. Mees, S. Dasari, J. Hejna, T. Kreiman, C. Xu *et al.*, “Octo: An open-source generalist robot policy,” *arXiv preprint arXiv:2405.12213*, 2024.
- [5] M. J. Kim, C. Finn, and P. Liang, “Fine-tuning vision-language-action models: Optimizing speed and success,” *arXiv preprint arXiv:2502.19645*, 2025.
- [6] M. M. Veloso, “Flexible strategy learning: Analogical replay of problem solving episodes,” *city*, vol. 3, p. a3, 1994.
- [7] Y. J. Ma, S. Sodhani, D. Jayaraman, O. Bastani, V. Kumar, and A. Zhang, “Vip: Towards universal visual reward and representation via value-implicit pre-training,” *arXiv preprint arXiv:2210.00030*, 2022.
- [8] A. George, S. Gano, P. Katragadda, and A. B. Farimani, “Vital pretraining: Visuo-tactile pretraining for tactile and non-tactile manipulation policies,” *arXiv preprint arXiv:2403.11898*, 2024.
- [9] A. George and A. B. Farimani, “One act play: Single demonstration behavior cloning with action chunking transformers,” *arXiv preprint arXiv:2309.10175*, 2023.
- [10] S. Gano, A. George, and A. B. Farimani, “Low fidelity visuo-tactile pretraining improves vision-only manipulation performance,” *arXiv preprint arXiv:2406.15639*, 2024.
- [11] Y. J. Ma, V. Kumar, A. Zhang, O. Bastani, and D. Jayaraman, “Liv: Language-image representations and rewards for robotic control,” in *International Conference on Machine Learning*. PMLR, 2023, pp. 23 301–23 320.
- [12] S. Nair, A. Rajeswaran, V. Kumar, C. Finn, and A. Gupta, “R3m: A universal visual representation for robot manipulation,” *arXiv preprint arXiv:2203.12601*, 2022.
- [13] J. Kirkpatrick, R. Pascanu, N. Rabinowitz, J. Veness, G. Desjardins, A. A. Rusu, K. Milan, J. Quan, T. Ramalho, A. Grabska-Barwinska *et al.*, “Overcoming catastrophic forgetting in neural networks,” *Proceedings of the national academy of sciences*, vol. 114, no. 13, pp. 3521–3526, 2017.
- [14] L. Zha, Y. Cui, L.-H. Lin, M. Kwon, M. G. Arenas, A. Zeng, F. Xia, and D. Sadigh, “Distilling and retrieving generalizable knowledge for robot manipulation via language corrections,” in *2024 IEEE International Conference on Robotics and Automation (ICRA)*. IEEE, 2024, pp. 15 172–15 179.
- [15] A. Car, S. S. Yarlagadda, A. Bartsch, A. George, and A. B. Farimani, “Plato: Planning with llms and affordances for tool manipulation,” *arXiv preprint arXiv:2409.11580*, 2024.
- [16] M. Kwon, H. Hu, V. Myers, S. Karamcheti, A. Dragan, and D. Sadigh, “Toward grounded commonsense reasoning,” in *2024 IEEE International Conference on Robotics and Automation (ICRA)*. IEEE, 2024, pp. 5463–5470.
- [17] J. Piaget, *Play, dreams and imitation in childhood*. Routledge, 2013.
- [18] A. N. Meltzoff and M. K. Moore, “Imitation of facial and manual gestures by human neonates,” *Science*, vol. 198, no. 4312, pp. 75–78, 1977.
- [19] T. Zhang, Z. McCarthy, O. Jow, D. Lee, X. Chen, K. Goldberg, and P. Abbeel, “Deep imitation learning for complex manipulation tasks from virtual reality teleoperation,” in *2018 IEEE international conference on robotics and automation (ICRA)*. IEEE, 2018, pp. 5628–5635.
- [20] B. C. Stadie, P. Abbeel, and I. Sutskever, “Third-person imitation learning,” *arXiv preprint arXiv:1703.01703*, 2017.

- [21] Y. Duan, M. Andrychowicz, B. Stadie, O. Jonathan Ho, J. Schneider, I. Sutskever, P. Abbeel, and W. Zaremba, "One-shot imitation learning," *Advances in neural information processing systems*, vol. 30, 2017.
- [22] A. Bartsch, A. Car, C. Avra, and A. B. Farimani, "Sculptdiff: Learning robotic clay sculpting from humans with goal conditioned diffusion policy," in *2024 IEEE/RSJ International Conference on Intelligent Robots and Systems (IROS)*. IEEE, 2024, pp. 7307–7314.
- [23] S. Young, D. Gandhi, S. Tulsiani, A. Gupta, P. Abbeel, and L. Pinto, "Visual imitation made easy," in *Conference on Robot learning*. PMLR, 2021, pp. 1992–2005.
- [24] J. Pari, N. M. Shafiullah, S. P. Arunachalam, and L. Pinto, "The surprising effectiveness of representation learning for visual imitation," *arXiv preprint arXiv:2112.01511*, 2021.
- [25] A. O'Neill, A. Rehman, A. Maddukuri, A. Gupta, A. Padalkar, A. Lee, A. Pooley, A. Gupta, A. Mandekar, A. Jain *et al.*, "Open x-embodiment: Robotic learning datasets and rt-x models: Open x-embodiment collaboration 0," in *2024 IEEE International Conference on Robotics and Automation (ICRA)*. IEEE, 2024, pp. 6892–6903.
- [26] M. Oquab, T. Darcet, T. Moutakanni, H. Vo, M. Szafraniec, V. Khalidov, P. Fernandez, D. Haziza, F. Massa, A. El-Nouby *et al.*, "Dinov2: Learning robust visual features without supervision," *arXiv preprint arXiv:2304.07193*, 2023.
- [27] X. Zhai, B. Mustafa, A. Kolesnikov, and L. Beyer, "Sigmoid loss for language image pre-training," in *Proceedings of the IEEE/CVF international conference on computer vision*, 2023, pp. 11 975–11 986.
- [28] D. M. Ziegler, N. Stiennon, J. Wu, T. B. Brown, A. Radford, D. Amodei, P. Christiano, and G. Irving, "Fine-tuning language models from human preferences," *arXiv preprint arXiv:1909.08593*, 2019.
- [29] J. Bohg, K. Hausman, B. Sankaran, O. Brock, D. Kragic, S. Schaal, and G. S. Sukhatme, "Interactive perception: Leveraging action in perception and perception in action," *IEEE Transactions on Robotics*, vol. 33, no. 6, pp. 1273–1291, 2017.